Synthesis and characterizations of benzothiadiazole-based fluorophores as potential wavelength-shifting materials

Yilin Li [a,b], Louis Scudiero [c], Tianhui Ren [a], Wen-Ji Dong [b,*]

[a] School of Chemistry and Chemical Engineering, Shanghai Jiao Tong University, Shanghai 200240, China
[b] Voiland School of Chemical Engineering and Bioengineering and Department of Veterinary & Comparative Anatomy, Pharmacology & Physiology, College of Veterinary Medicine; Washington State University, Pullman, WA 99164, USA
[c] Department of Chemistry and Materials Science and Engineering, Washington State University, Pullman, WA 99164, USA

ABSTRACT

The synthesized benzothiadiazole-based series fluorophores as potential wavelength-shifting materials exhibit large Stokes shifts (>160 nm) with multiple broad absorbance bands from UV region to 600 nm and a strong fluorescence peak around 700 nm (in CHCl$_3$). Intramolecular charge transfer (ICT) characters of the synthesized compounds are examined using UV–vis and photoluminescence solvatochromic shift measurements. Among the synthesized compounds, the fluorophores with asymmetrical structures exhibit larger Stokes shifts than those with symmetrical structures due to large dipole moment changes upon excitation. The fluorophores with electron-donating methoxyl groups attached to the triphenylamine donors are found to have strong ICT properties. Photophysical experimental results are supported by theoretical calculations using Density Function Theory (DFT) and Time Dependent Density Function Theory (TD-DFT) methods. Calculated frontier molecular orbitals (MOs) of ground states on these fluorophores showed an increase in ICT character up to 50% from HOMO to LUMO. Geometric optimization calculations of the excited state reveal that these fluorophores show a more planar structure for the excited state than the ground state, which allows more π–π^* overlap and leads to larger Stokes shifts and higher quantum yields.

Published by Elsevier B.V.

1. Introduction

Conjugated organic compounds have been extensively explored in many fields of science [1]. Their special ability to transfer light from lower wavelength to higher wavelength makes them unique materials applied in organic light-emitting diodes [2], organic photovoltaics [3–5] and biochemical sensors [6]. Because of unique spectroscopic properties associated with some of these compounds, they can also be used as wavelength-shifting materials to increase solar energy transfer efficiency of plant photosynthesis and some man-made solar cells [7–9]. For example, many photovoltaic materials, particularly cadmium telluride (CdTe), exhibit a poor spectral response to short wavelength light, which means that an appreciable fraction of incident photon energy is lost during energy conversion. One approach to improving the energy conversion efficiency at short wavelength (<500 nm) is to modify the spectrum that is incident on the surface of photovoltaic materials by placing a layer of a wavelength-shifting material in front of the photovoltaic device. The wavelength-shifting material absorbs short wavelength photons and re-emits photons at longer, more favorable wavelengths before they reach the photovoltaic device. To achieve significant enhancement in energy conversion efficiency of photovoltaic device using wavelength-shifting materials, it is desirable to have materials with spectral properties of absorption at full UV range and emission at 680–700 nm. This means that these materials should have large Stokes shifts (>150 nm) with high quantum yield to avoid self-quenching and energy loss [10]. The π-conjugated organic compounds are good candidates for wavelength-shifting material development.

Recent functional and structural studies on π-conjugated compounds have revealed the correlations between their spectroscopic properties and structures [11–13]. Different methods have been used to tune the spectral properties of π-conjugated compounds such as increasing the molecular conjugation to make the absorption spectra red shift [14], tuning the intramolecular charge transfer (ICT) character to shift the emission spectra [15] and building energy-transfer system to obtain large Stokes shift [16].

In addition, recent studies have shown that small organic molecules with benzothiadiazole structure exhibit large Stokes shifts with high quantum yields and red light-emitting properties. These benzothiadiazole-based materials have been widely employed in photovoltaic applications [17–20]. Furthermore,

* Corresponding author. Tel.: +1 509 335 5798.
  E-mail address: wdong@vetmed.wsu.edu (W.-J. Dong).

recent report revealed that benzothiadiazole in these compounds showed charge-acceptor properties [21]. Also, it is known that triphenylamine-based derivatives are electron-rich molecules that can be introduced as donor to increase the ICT character [15]. Therefore, constructing a benzothiadiazole-triphenylamine based ICT system can be a useful approach to tuning the photophysical properties of benzothiadiazole-based compounds to meet the specific requirements of wavelength-shifting materials.

To develop these π-conjugated compounds with desired photophysical properties, we synthesized a series of fluorophores containing benzothiadiazole core structure linked to triphenylamines with different functional groups. In addition to their specific intrinsic photophysical properties, the synthesized fluorophores exhibit large Stokes shifts with multiple broad absorbance bands from the UV region to 600 nm and a strong fluorescence band around 700 nm (in $CHCl_3$). Theoretical computational studies of these compounds not only revealed strong ICT during their photo-excitation, but also provide information on the relationship between their photophysical properties and structures.

2. Experimental

2.1. Spectroscopic measurements

Absorption spectra were recorded with a Bechman Coulter DU730 Life Science UV-Vis spectrophotometer. Absorption spectra of the compounds above 250 nm were presented in this study. The abrupt changes in absorption at 340 nm were caused by instrumental artifact primarily due to automatic lamp switch during spectral measurements. Emission spectra were collected on an ISS PC1 photon counting spectrofluorometer using the lowest absorption maximum as the excitation wavelength. Fluorescence lifetimes were measured in the hexane solution on a HORIBA JOBIN YVON fluorocube using a LED 459 nm for compound **1** or LED 495 nm for **1a–d** as excitation light source. The relative fluorescence quantum yields were determined in the hexane solution using perylene (0.94, $\lambda_{ex} = 435$ nm) as standard for compound **1** and then using compound **1** (0.59, $\lambda_{ex} = 475$ nm) as standard for compounds **1a–d**. The fluorescence quantum yield was calculated by [22]:

$$\Phi_x = \Phi_{st} \left(\frac{\text{Grad}_x}{\text{Grad}_{st}} \right) \left(\frac{n_x}{n_{st}} \right)^2$$

Where the subscripts *st* and *x* denote standard and sample respectively, Φ is the fluorescence quantum yield, Grad is the gradient from the plot of integrated fluorescence intensity vs. absorbance, and *n* is the refractive index of the solvent. The fluorescence lifetime decays obtained from time-resolved measurements were fitted with the one-exponential decay equation:

$$I(t) = Ae^{-t/\tau_f}$$

2.2. Computational methods

The S_0 and S_1 geometries of **1a–d** were optimized using B3LYP/6-31G(d). For the excited state, TD-DFT with B3LYP function was used on the optimized structures. All calculations were performed with Gaussian 09 package [23].

2.3. Synthesis and characterization

Unless otherwise noted, all reagents were used as received and without further purification. Chromatography was carried out with 60–200 mesh silica gel for flash columns. ^{1}H NMR spectra and ^{13}C NMR were collected on a 300 MHz spectrometer at room temperature. Mass spectra were recorded on a 4800 MALDI TOF/TOF

analyzer. C, H & N percentage analyses were carried out on **1a–d** to prove that these compounds were pure enough for the fluorescence measurements.

General procedure of palladium complex catalytic reaction: A mixture of reactants, base and Pd-catalyst in toluene was refluxed for 24 h. The resulting mixture was filtered, washed by water and extracted by DCM three times. The combined organic layers were collected and dried over $MgSO_4$ anhydrous. After the solvent was removed under reduced pressure, the residue was purified by flash column chromatography on SiO_2 with hexane and ethyl acetate as eluant to obtain the desired product.

General procedure of NBS bromination: To a solution of reactant, NBS was added in small portions, and the reaction solution was stirred under room temperature for appropriate time. The resulting solution was filtered, washed by water and extracted by DCM three times. The combined organic layers were collected and dried over $MgSO_4$ anhydrous. After the solvent was removed under reduced pressure, the residue was purified by flash column chromatography on SiO_2 with hexane and ethyl acetate as eluant to obtain the desired product.

2.3.1. 4,7-di(thiophen-2-yl)benzo[c][1,2,5]thiadiazole (1)

Red solid (1.6 mg, yield 78.3%). $R_f = 0.33$ (Hex: EA = 15: 1). ^{1}H NMR (300 MHz, $CDCl_3$, δ): 8.13 (dd, 2H, J = 3.7 Hz), 7.88 (s, 2H), 7.47 (dd, 2H, J = 5.1 Hz), 7.23 (dd, 2H, J = 5.1 Hz).

2.3.2. 4,7-bis(5-bromothiophen-2-yl)benzo[c][1,2,5]thiadiazole (3b)

Dark red solid (2.1 g, yield 86.1%). $R_f = 0.47$ (Hex: EA = 15: 1). ^{1}H NMR (300 MHz, $CDCl_3$, δ): 7.82 (d, 2H, J = 4.0 Hz), 7.80 (s, 2H), 7.17 (d, 2H, J = 4.0 Hz).

2.3.3. Bis(4-methoxylphenyl)amine (5)

White solid (6.0 g, yield 98.0%). $R_f = 0.30$ (Hex: EA = 5: 1). ^{1}H NMR (300 MHz, $CDCl_3$, δ): 6.96 (d, 4H, J = 8.9 Hz), 6.84 (d, 4H, J = 8.9 Hz), 5.28 (s, 1H), 3.78 (s, 6H).

2.3.4. 4-bromo-N,N-bis(4-methoxylphenyl)aniline (6)

White solid (2.2 g, yield 65.6%). $R_f = 0.26$ (Hex: EA = 5: 1). ^{1}H NMR (300 MHz, $CDCl_3$, δ): 7.27 (d, 2H, J = 9.1 Hz), 7.08 (d, 4H, J = 9.1 Hz), 6.87–6.81 (m, 6H), 3.81 (s, 6H).

2.3.5. 4-methoxyl-N-(4-methoxylphenyl)-N-(4-(4,4,5,5-tetramethyl-1,3,2-dioxaborolan-2-yl)phenyl)aniline (4b)

White solid (1.1 g, yield 45.3%). $R_f = 0.18$ (Hex: EA = 5: 1). ^{1}H NMR (300 MHz, $CDCl_3$, δ): 7.61 (d, 2H, J = 8.7 Hz), 7.08 (d, 4H, J = 9.0 Hz), 6.88–6.81 (m, 6H), 3.80 (s, 6H), 1.32 (s, 12H). MS-MALDI: m/z calcd for $C_{26}H_{30}BNO_4^+$ 431.2268, found 431.2214.

2.3.6. N,N-diphenyl-4-(5-(7-(thiophen-2-yl)benzo[c][1,2,5]thiadiazol-4-yl)thiophen-2-yl)aniline (1a)

Red solid (145 mg, yield 50.6%). $R_f = 0.29$ (Hex: EA = 10: 1). ^{1}H NMR (300 MHz, $CDCl_3$, δ): 8.12 (d, 2H, J = 4.1 Hz), 7.88 (s, 2H), 7.58 (d, 2H, J = 8.7 Hz), 7.47 (dd, 1H, J = 5.1 Hz), 7.34 (dd, 4H, J = 6.9 Hz), 7.23 (dd, 1H, J = 8.9 Hz), 7.16–7.03 (m, 9H). ^{13}C NMR (300 MHz, $CDCl_3$, δ): 123.5 123.7 124.9 125.3 126.1 126.8 127.0 128.2 129.0 129.6 147.6. MS-MALDI: m/z calcd for $C_{32}H_{21}N_3S_3^+$ 543.0898, found 543.1697. Anal. (%): calcd (found) for $C_{32}H_{21}N_3S_3$: C 70.69(68.02), H 3.89(3.62), N 7.73(7.23).
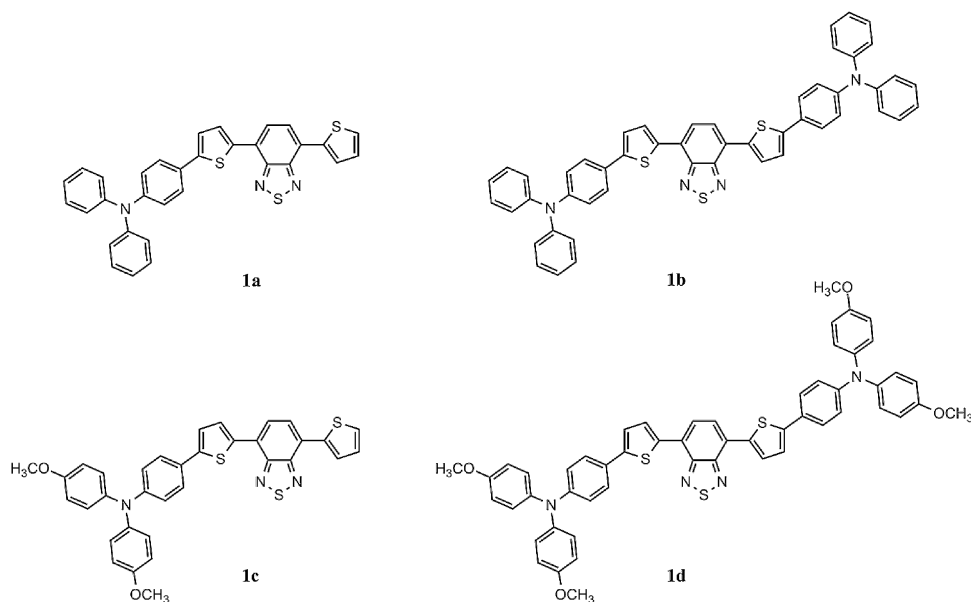
Fig. 1. Molecular structures of compounds **1a–d**.

2.3.7. 4,4′-(5,5′-(benzo[c][1,2,5]thiadiazole-4,7-diyl)bis(thiophene-5,2-diyl))bis(N,N-diphenylaniline) (**1b**)

Dark red solid (365 mg, yield 42.5%). $R_f = 0.28$ (Hex: EA = 5: 1). ^{1}H NMR (300 MHz, CDCl$_3$, δ): 8.07 (d, 2H, $J = 3.9$ Hz), 7.79 (s, 2H), 7.56 (d, 4H, $J = 11.1$ Hz), 7.31 (t, 8H), 7.16–7.03 (m, 18H). ^{13}C NMR (300 MHz, CDCl$_3$, δ): 123.5 123.7 124.9 125.5 126.8 128.3 128.9 129.6 147.6. MS-MALDI: m/z calcd for C$_{50}$H$_{34}$N$_4$S$_3$$^+$ 786.1946, found 786.1304. Anal. (%): calcd (found) for C$_{50}$H$_{34}$N$_4$S$_3$: C 76.30(79.45), H 4.35(4.59), N 7.12(6.11).

2.3.8. 4-methoxyl-N-(4-methoxylphenyl)-N-(4-(5-(7-(thiophen-2-yl)benzo[c][1,2,5]thiadiazol-4-yl)thiophen-2-yl)phenyl)aniline (**1c**)

Dark red solid (75 mg, yield 23.6%). $R_f = 0.31$ (Hex: EA = 5: 1). ^{1}H NMR (300 MHz, CDCl$_3$, δ): 8.12 (d, 2H, $J = 3.9$ Hz), 7.87 (dd, 2H, $J = 1.9$ Hz), 7.52 (d, 2H, $J = 8.7$ Hz), 7.46 (dd, 1H, $J = 5.1$ Hz), 7.29 (d, 1H, $J = 4.0$ Hz), 7.23 (dd, 1H, $J = 8.9$ Hz), 7.11 (d, 4H, $J = 8.9$ Hz), 6.96 (d, 2H, $J = 10.7$ Hz), 6.87 (d, 4H, $J = 8.9$ Hz), 3.81 (s, 6H). ^{13}C NMR (300 MHz, CDCl$_3$, δ): 55.7 115.0 120.4 122.9 125.2 125.6 126.1 126.3 126.7 126.9 127.0 127.5 128.2 129.1 137.4 139.7 140.7 146.2 148.8 152.7 152.9 156.4. MS-MALDI: m/z calcd for C$_{34}$H$_{25}$N$_3$O$_2$S$_3$$^+$ 603.1109, found 603.1437. Anal. (%): calcd (found) for C$_{34}$H$_{25}$N$_3$O$_2$S$_3$: C 67.63(68.08), H 4.17(4.03), N 6.96(6.85).

2.3.9. 4,4′-(5,5′-(benzo[c][1,2,5]thiadiazole-4,7-diyl)bis(thiophene-5,2-diyl))bis(N,N-bis(4-methoxylphenyl)aniline) (**1d**)

Dark red solid (251 mg, yield 63.4%). $R_f = 0.48$ (Hex: EA = 2: 1). ^{1}H NMR (300 MHz, CDCl$_3$, δ): 8.09 (d, 2H, $J = 3.9$ Hz), 7.83 (s, 2H), 7.51 (d, 4H, $J = 8.7$ Hz), 7.28 (d, 2H, $J = 3.8$ Hz), 7.11 (d, 8H, $J = 8.9$ Hz), 6.96 (d, 4H, $J = 6.8$ Hz), 6.87 (d, 8H, $J = 8.9$ Hz), 3.81 (s, 12H). ^{13}C NMR (300 MHz, CDCl$_3$, δ): 55.7 115.0 120.5 122.9 125.3 125.8 126.3 126.7 127.0 128.9 137.6 140.8 146.0 148.7 152.8 156.3. MS-MALDI: m/z calcd for C$_{54}$H$_{42}$N$_4$O$_4$S$_3$$^+$ 906.2368, found 906.2276. Anal. (%): calcd (found) for C$_{54}$H$_{42}$N$_4$O$_4$S$_3$: C 71.50(70.16), H 4.67(4.42), N 6.18(6.09).

3. Results and discussion

3.1. Molecular structures and synthesis

Compounds **1a–d** (Fig. 1) are all benzothiadiazole-based fluorophores with different triphenylamine (TPA) functionalities. They can be classified by their asymmetrical (**1a** and **1c**) or symmetrical (**1b** and **1d**) structures and the absence of methoxyl groups (**1a** and **1b**) or the presence of methoxyl groups (**1c** and **1d**) which serve as electron-donating groups. Compound **1b** has been reported before [24] and is herein used as a comparison of other compounds.

The synthesis of compounds **1a–d** from 4,7-dibromobenzo[c][1,2,5]thiadiazole (**2**) is depicted in Scheme 1. A modified previously reported procedure is used to synthesize compound **1** without further purification [25]. Compounds **3a** and **3b** are obtained by the selective bromination [15,26] on the thiophene group of compound **1**. Compound **4b** is synthesized from two step Buchwald–Hartwig coupling [27,28] followed by the reaction with B$_2$(pin)$_2$ [29,30]. The compounds **3a** and **3b** reacting with 4-(Diphenylamino)phenylboronic acid **4a** or **4b** under palladium complex catalyst lead to products **1a–d**. Compounds **1a** and **1c** are red solid and are both donor–acceptor (DA) type fluorophores while compounds **1b** and **1c** are dark-red solid and donor–acceptor–donor (D$_2$A) type fluorophores.

3.2. Characterization of photophysical properties

Photophysical properties of these compounds were investigated by spectroscopic measurements. Fig. 2 shows the absorption and emission spectra of compounds **1a–d** in chloroform, and the pertinent photophysical parameters are summarized in Table 1. In our measurements, tetra-N-phenylbenzidine (TPB) and compound **1** are used as references to investigate the ICT character of compounds **1a–d**.

Without conjugation to TPA, compound **1** in chloroform exhibits a strong fluorescence at 565 nm and a multiple-band absorbance with major maximal peaks at 300 nm and 445 nm, respectively. This results in a 120 nm Stokes shift (Fig. 2 left). Upon conjugation to TPA derivatives, high energy absorption bands of compounds **1a–d** are
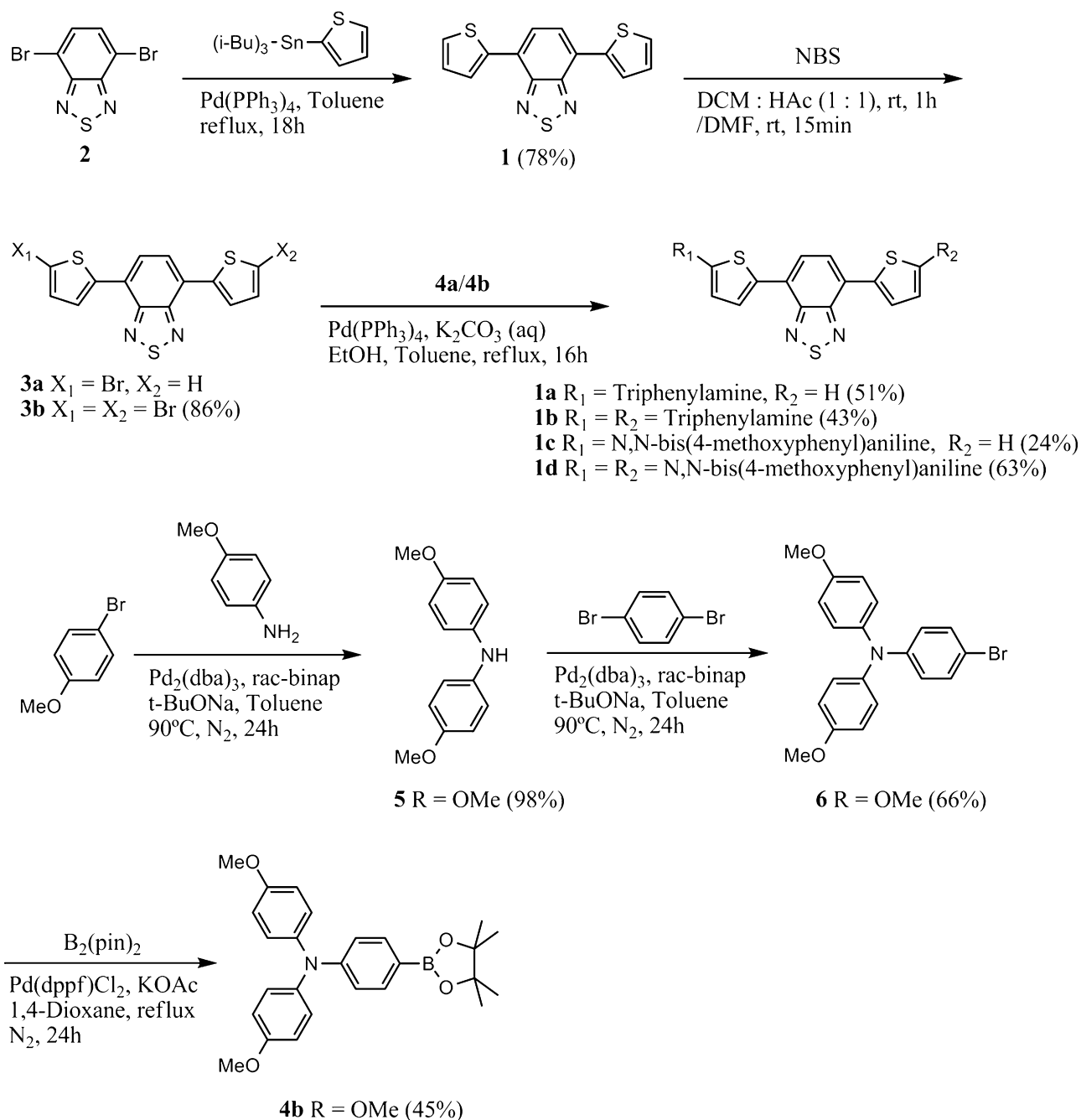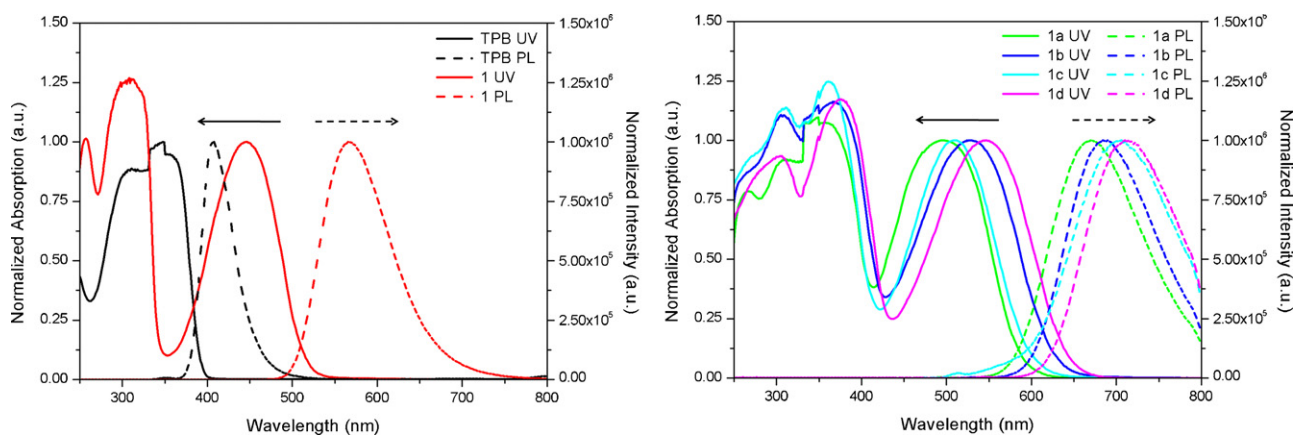
Scheme 1. Synthesis route of compounds **1a–d**.

Table 1
Photophysical parameters of compounds **1** and **1a–d** including absorption (λ_{abs}), molar absorption coefficient (ε) and emission (λ_{em}) maximum, Stokes shift ($\lambda_{em} - \lambda_{abs}$), fluorescence quantum yield (Φ_f) and lifetime (τ_f), radiative (k_r) and nonradiative (k_{nr}) rate constants.

Compound	λ_{abs} (nm)[a]	ε (M^{-1} cm^{-1})	λ_{em} (nm)[b]	Stokes shift (nm/cm^{-1})	Φ_f	τ_f (ns)	k_r (10^7 s^{-1})	k_{nr} (10^7 s^{-1})
1	445	8016	565	120/4800	0.59	10.24	5.76	4.00
1a	495	9007	670	175/5300	0.33	6.62	4.99	10.12
1b	530	15,185	690	160/4400	0.23	5.13	4.48	15.01
1c	510	15,082	705	195/5400	0.28	6.55	4.27	10.99
1d	545	18,804	710	165/4300	0.18	4.90	3.67	16.73

[a] Lower energy absorption maximum.
[b] Photoluminescence emission maximum, excited at λ_{abs} in chloroform.

Fig. 2. Normalized UV–vis absorption (solid lines) and photoluminescence (dashed lines) spectra. Left: TPB (λ_{ex} = 350 nm, black), **1** (λ_{ex} = 445 nm, red) in chloroform. Right: **1a** (λ_{ex} = 495 nm, green), **1b** (λ_{ex} = 530 nm, blue), **1c** (λ_{ex} = 510 nm, cyan) and **1d** (λ_{ex} = 545 nm, magenta) in chloroform. Note: the sharp changes observed in UV absorption at 340 nm are due to instrumental artifacts.

broadened and red-shifted with maximal peak at 375 nm. The low energy absorption bands are red-shifted to 495–545 nm. The molar absorption coefficients associated with the low energy absorption bands are also increased, which allows compounds **1a**–**d** to absorb more light than compound **1**. Emission spectra of these compounds are also red-shifted to 670–710 nm (Fig. 2 right). Conjugation to TPA increased Stokes shifts of the target compounds by 40–75 nm.

Each molecule of compounds **1a**–**d** can be considered as a donor–acceptor system, in which TPA derivatives serve as electron donors while the benzothiadiazole core structure serves as an electron acceptor. Typically, TPA derivatives (such as TPB) have strong absorbance from 250 nm to 400 nm (Fig. 2 left) and compound **1** also has a strong absorbance around 300 nm. Thus, the higher energy absorbance (250–400 nm) of compounds **1a**–**d** inherits UV absorbance spectral characteristics of both donor and acceptor and can be ascribed to the π–π^* transitions of the fluorophores [31]. The lower energy absorbance of these compounds at 500 nm is believed to be caused by electronic transition from donor to acceptor, which can be used to reveal the ICT character of the molecules. Furthermore, the red-shift observed in absorption and emission spectra of compounds **1a**–**d** suggests that molecules with the electron-donating methoxyl group (**1c**) or with one more conjugated group of TPA derivatives (**1b** and **1d**) will have better molecular conjugation. The observed large Stokes shifts (>160 nm) of these fluorophores may be the result of changes in molecular structure from the less planar geometry in their ground state to the more planar geometry at their excited state [32,33]. It is also noted that compounds **1a** and **1c** with asymmetrical structures show larger Stokes shift than compounds **1b** and **1d** with symmetrical structures. It is known that asymmetrical molecules display larger changes in dipole moments going from ground to excited states [34].

Further characterization of compounds **1** and **1a**–**d** with time-resolved fluorescence measurement allows the determination of the radiative and nonradiative rate constants using the following equations [35] (results are given in Table 1).
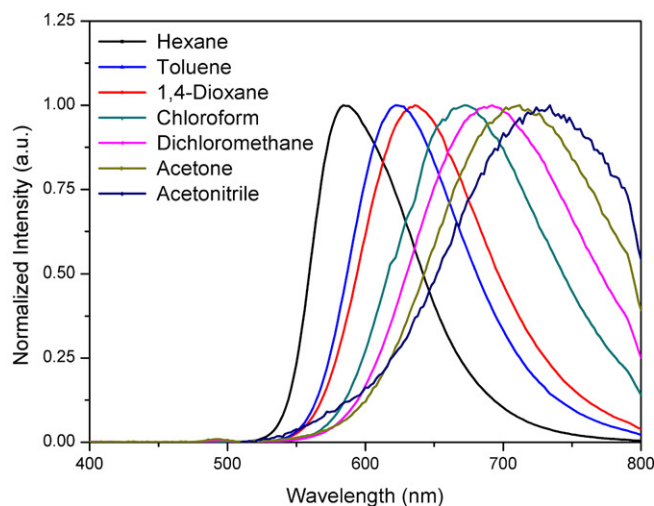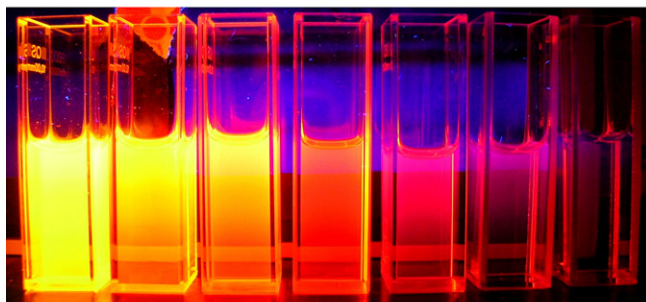
$$k_r = \frac{\Phi_f}{\tau_f}$$

$$k_{nr} = \frac{1 - \Phi_f}{\tau_f}$$

Without conjugation to TPA derivatives, compound **1** exhibits a quantum yield of 0.59 and a fluorescence lifetime of 10.24 ns. Radiative process (5.76×10^7 s^{-1}) can effectively compete with nonradiative process (4.00×10^7 s^{-1}) in the course of the relaxation of the excited state of the compound. Upon conjugation with TPA derivatives, the quantum yields and lifetimes decreased from 0.33 to 0.18 and from 6.62 ns to 4.90 ns, respectively. Calculated nonradiative rates (Table 1) suggest that the observed decrease in quantum yields and fluorescence lifetimes in the conjugated compounds are largely caused by dominating roles of rapid nonradiative processes that are significantly increased upon conjugation. The increase in the nonradiative process in these compounds is likely due to more freedom of internal structural rotation, which is consistent with the fact that compounds **1b** and **1d** have both symmetrical structure and more freedom of internal structural rotation. Therefore, compounds **1b** and **1d** show lower quantum yields and shorter fluorescence lifetimes than compounds **1a** and **1c**.

It is known that ICT plays an important role in tuning fluorescence spectral properties of π-conjugated compounds. Our spectroscopic study has shown that ICT occurs upon excitation of the fluorophores (Fig. 2). Because the ICT process is sensitive to environmental polarity and dipole moment of the molecules, the emission spectra of the fluorophores are expected to shift in response to different solvents, which can be used to investigate ICT properties of the fluorophores. In this study, we examine emission spectral changes of each fluorophore with different solvents. Fig. 3 shows fluorescence photography (left) and normalized emission spectral changes (right) of compound **1a** in various solvents with different polarities. With the increase in polarity of the solvents from hexane, toluene, 1,4-dioxane, chloroform, dichloromethane, acetone to acetonitrile, the fluorescent color of sample solution containing **1a** changes from yellow to deep red. Furthermore, brightness or intensity of sample **1a** decreases with increasing solvent polarity. The decrease in fluorescence intensity is largely caused by strong dipole–dipole interaction between fluorophore and solvent molecules, which increases solvent relaxation time upon fluorophore excitation and expedites nonradiative process. Due to a strong dipole–dipole interaction between fluorophore and solvent molecules, the observed spectral changes are the result of changes in dipole moments between the delocalized ground state and the highly localized excited state of the fluorophore. The highly localized excited state is believed to be caused by ICT from the donor component to the acceptor component of the molecule. Relationship between emission wavelength and the difference in the

Fig. 3. Equimolar fluorescence photography (left) and solvatochromic shift (right) of compound **1a** with different solvents (from left to right): hexane, toluene, 1,4-dioxane, chloroform, dichloromethane, acetone and acetonitrile.

dipole moment of typical CT compounds can be expressed by the Lippert–Mataga equation [36–38].

$$\widetilde{\upsilon}_{flu}^{CT} = \widetilde{\upsilon}_{flu}^{vac} - \frac{2\overrightarrow{\mu}_e(\overrightarrow{\mu}_e - \overrightarrow{\mu}_g)}{hca_0^3}\left[\frac{\in - 1}{2\in + 1} - \frac{1}{2}\left(\frac{n^2-1}{n^2+1}\right)\right]$$

$$\Delta f = \frac{\in - 1}{2\in + 1} - \frac{1}{2}\left(\frac{n^2-1}{2n^2+1}\right)$$

where $\widetilde{\upsilon}_{flu}^{CT}$ is the emission wavenumber excited at the ICT absorption peak and $\widetilde{\upsilon}_{flu}^{vac}$ in the gas phase; $\overrightarrow{\mu}_g$ and $\overrightarrow{\mu}_e$ is the dipole moment in the ground state and excited state, respectively; h is the Planck's constant and c is the speed of light in vacuum; a_0 is the radius of Onsagar's cavity around a fluorophore; $\in$ is the dielectric constant; n is refractive index $\in$ and n can be expressed by Δf, which represents the effect of solvent. It should be noted that this equation contains many assumptions. For example, the fluorophore is assumed to be spherical, and there is no consideration of specific interactions with the solvent. Furthermore, this equation ignores the polarizability of the fluorophore and assumes that the ground and excited state dipole moments orient in the same direction.

Fig. 4 shows Lippert–Mataga plots to illustrate the relationship of spectral shifts (given in wavenumbers) of the fluorophores **1a–d** and solvent polarity (represented by Δf). The results show that compounds **1a** and **1b** exhibit linear decrease of emission wavenumber with Δf (Fig. 4), suggesting that the dipole moment of the excited state of the fluorophores is larger than the dipole moment of the ground state. Lippert–Mataga plots of **1c** and **1d** (solid lines in Fig. 4) obtained from measurements in all solvents show poor linear relationship. This can be explained by the para position of the methoxyl group of TPA which alters the electronic distribution of the molecular conjugation in the ground state and forms hydrogen bond with higher polar solvent molecules. This explanation is supported by measurements performed in the solvents with low or medium polarities, in which the wavenumbers of compounds **1c** and **1d** decreased linearly as Δf increased (dashed lines in Fig. 4). The observed results from Lippert–Mataga plots of **1a–d** definitely reveal the ICT occurrence during the excitation of these fluorophores.

3.3. Quantum chemistry computation

To further understand the electronic properties of the ground and excited states of the synthesized fluorophores, we performed quantum chemistry computations on compounds **1a–d**. Ground state (S_0) geometric optimizations on **1a–d** were first performed at the B3LYP/6-31G(d) level of DFT theory without symmetry constraints. Molecular orbital calculations based on the optimized S_0 geometries of **1a–d** were then carried out. The computational results show that HOMOs are located on both donor and acceptor groups while LUMOs are only located on the acceptors. These results are consistent with observed photophysical data and Lippert–Mataga plots of solvatochromic shift that show that ICT occurred upon the excitation. The localized LUMOs suggest that the benzothiadiazole core structure serves as acceptor upon ICT occurrence. The energy of HOMO and LUMO and orbital contributions of donor and acceptor are given in Table 2.

Compounds **1a–d** have electronically delocalized HOMO in the ground states, to which electron contributions are 56–73% from donor groups and 27–44% from acceptor groups. In contrast, the highly localized LUMO is dominantly contributed by acceptor electrons (>94%), which is likely caused by ICT from the ground state to the excited state of the fluorophores. The calculated frontier orbitals (HOMO and LUMO) are shown pictorially in Fig. 5, where the HOMO and LUMO are considered to be largely π and π* orbitals. Compared to compounds **1a** and **1b**, compounds **1c** and **1d** show a decrease in electron contribution in their HOMO from acceptor groups to the molecular orbitals due to the presence of the methoxyl group, which causes an enriched electron density in the donor group. It is noted that electron contribution to the LUMO from donors of symmetrical structures (**1b** and **1d**) was doubled compared to the asymmetrical ones (**1a** and **1c**) because of the D$_2$A type nature of the fluorophores. Furthermore, the calculated energy gaps between HOMO and LUMO (HLG) of compounds **1a–d** (Table 2), which are correlated to the lower excitation energy of the fluorophores, are consistent with the experimental observations (i.e., the excitation wavelengths of compounds **1a–d** shifted to red with the decrease of HLG) (Table 2).

The ICT property can be characterized the difference in the electronic contribution of acceptor to LUMO and HOMO (shown in Table 2). Our results suggest that the observed energy transitions are π–π* with more than 50% charge transfer characteristics (**1a**:
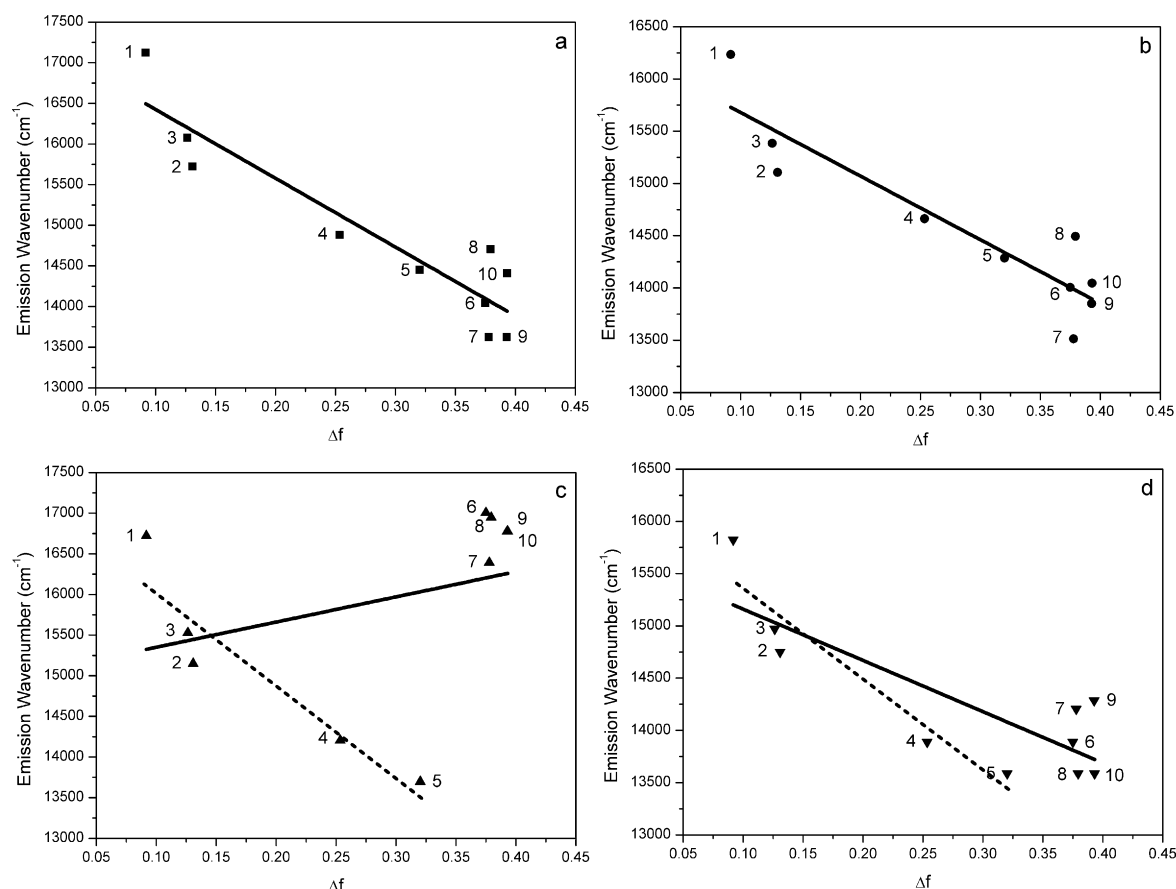
Fig. 4. Lippert–Mataga plots for compounds **1a–d**. Solvent: 1 (hexane, Δf=0.092), 2 (1,4-dioxane, Δf=0.131), 3 (toluene, Δf=0.126), 4 (chloroform, Δf=0.254), 5 (dichloromethane, Δf=0.320), 6 (acetone, Δf=0.375), 7 (DMF, Δf=0.378), 8 (ethanol, Δf=0.379), 9 (acetonitrile, Δf=0.393), 10 (methanol, Δf=0.393). Solid line: linear fit in the whole Δf range for **1a–d**. Dashed line: linear fit in the low or medium Δf range for **1c–d**.

Table 2
HOMO and LUMO energy and orbital contributions (%) of donor and acceptor in compounds **1a–d**.

	HOMO			LUMO			HLG[a]	Ex. W. (exp)[b]
	Donor	Acceptor	eV	Donor	Acceptor	eV	eV	nm/eV
1a	61%	39%	−4.480	3%	97%	−2.560	2.280	495/2.505
1b	56%	44%	−4.650	6%	94%	−2.546	2.104	530/2.339
1c	73%	27%	−4.612	3%	97%	−2.480	2.132	510/2.431
1d	64%	36%	−4.387	6%	94%	−2.394	1.993	545/2.275

[a] HLG: HOMO–LUMO gap = LUMO − HOMO.
[b] Excitation wavelength, equals to absorption wavelength at lowest energy.

58%; **1b**: 50%; **1c**: 70%; **1d**: 50%). In addition, the compound **1c** has more charge transfer character than the others due to more electrons on donor group within the conjugated structure.

To further characterize the properties of spectral transitions of the synthesized fluorophores, we utilized TD-DFT to examine the molecular geometries of the ground states (S_0) and the excited states (S_1) of compounds **1a–b**. The results are shown in Fig. 6 and Table 3. Although the calculated dihedral difference between S_0 and S_1 states of **1b** is smaller than that of **1a**, more energy loss in the internal structural rotation during the excitation is expected for compound **1b** than that for compound **1a** since **1b** has one more donor group than **1a**. Furthermore, **1a** shows more planar structure in its S_1 state, which allows the transition of the electron from donor to acceptor efficiently and leads to higher quantum yield (e.g., **1a**: 0.33 > **1b**: 0.23). In addition, the molecule with larger

geometric difference between S_0 and S_1 states has a large Stokes shift (e.g., **1a**: 175 nm > **1b**: 160 nm) due to longer relaxing time during the excitation, which is supported by their lifetime results (e.g., **1a**: 6.62 ns > **1b**: 5.13 ns). Computations on compounds **1c** and **1d** were not performed due to extensive cost of computational time. However, due to structural similarity, we predict similar behavior for these compounds.

Table 3
Dihedral angles between donor (TPA) and acceptor (**1**) in optimized S_0 and S_1 geometries of **1a**.

Compound	S_0 dihedral (°)	S_1 dihedral (°)	$S_0 − S_1$ dihedral (°)
1a	23.2	5.6	17.6
1b	24.0	10.0	14.0

HOMO | LUMO

1a

1b

1c

1d
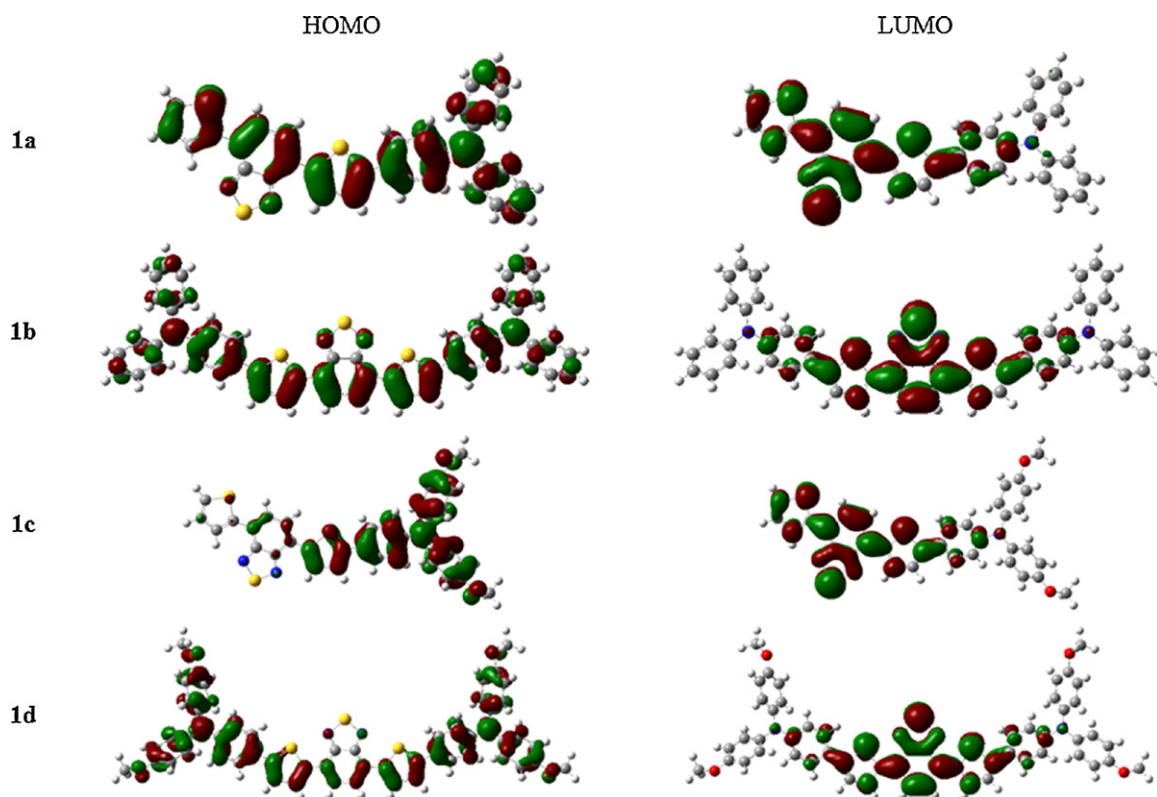
Fig. 5. Frontier Orbitals for **1a–d**.

S_0 | S_1

1a

1b
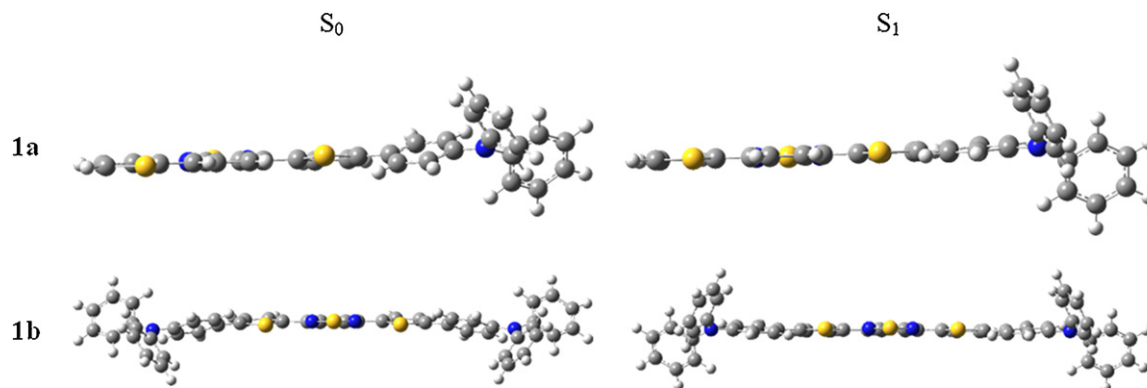
Fig. 6. S_1 and S_2 geometrical structures of **1a** and **1b**.

4. Conclusion

In conclusion, a series of benzothiadiazole-based fluorophores including benzothiadiazole core structure and different TPA functionalities have been synthesized. All of the fluorophores exhibit large Stokes shifts (>160 nm) with multiple broad absorbance bands from UV region to 600 nm and a strong fluorescence peak around 700 nm (in CHCl$_3$). Examination of the photophysical properties of these fluorophores suggest that TPA derivatives serve as donor and benzothiadiazole as acceptor in these compounds. The solvatochromic shifts of **1a–d** on the basis of ICT mechanism also were investigated. The emission spectra shift to red due to the introduction of an electron-donor group to the donor (**1a** vs. **1c** or **1b** vs. **1d**) and the addition of one more conjugated group of TPA derivatives (**1a** vs. **1b** or **1c** vs. **1d**) to the molecules. Our study also showed that the fluorophores with asymmetrical

structures exhibit larger Stokes shifts and higher quantum yields due to the larger dipole moment change from the ground state to the excited state and a more planar S$_1$ state which reduces the internal rotation. DFT and TD-DFT calculations support the photophysical experimental results by showing that lower HLG leads to a red-shift of the emission wavelength and ICT occurs from delocalized HOMO to localized LUMO. These specific photophysical properties of compounds **1a–d** make them good candidates for potential wavelength-shifting materials. However, it is noted that fluorescence quantum yields of the synthesized compounds are range from 0.18 to 0.33, which may limit applications of these compounds. The further efforts of our research will be made to improve fluorescence quantum yields by fine tune molecular structures of the compounds. We will study the wavelength-shifting properties of these compounds in their solid state, particularly in solid film on a surface of man-made CdTe solar cells. It is expected

that changes in medium environment of the compounds may significantly changes in the fluorescence quantum yields and other photophysical properties of the molecules.

Acknowledgments

Appendix A. Supplementary data

Supplementary data associated with this article can be found, in the online version, at doi:10.1016/j.jphotochem.2012.01.011.

References

[1] S.R. Forrest, M.E. Thompson, Introduction: organic electronics and optoelectronics, Chem. Rev. 107 (2007) 923–925.
[2] A.C. Grimsdale, K.L. Chan, R.E. Martin, P.G. Jokisz, A.B. Holmes, Synthesis of light-emitting conjugated polymers for applications in electroluminescent devices, Chem. Rev. 109 (2009) 897–1091.
[3] Y.J. Cheng, S.H. Yang, C.S. Hsu, Synthesis of conjugated polymers for organic solar cell applications, Chem. Rev. 109 (2009) 5868–5923.
[4] P. Heremans, D. Cheyns, B.P. Rand, Strategies for increasing the efficiency of heterojunction organic solar cells: material selection and device architecture, Acc. Chem. Res. 42 (2009) 1740–1747.
[5] N. Martin, L. Sanchez, M.A. Herranz, B. Illescas, D.M. Guldi, Electronic communication in tetrathiafulvalene (TTF)/C60 systems: toward molecular solar energy conversion materials? Acc. Chem. Res. 40 (2007) 1015–1024.
[6] S.W. Thomas III, G.D. Joly, T.M. Swager, Chemical sensors based on amplifying fluorescent conjugated polymers, Chem. Rev. 107 (2007) 1339–1386.
[7] E. Espi, A. Salmeron, A. Fontecha, Y. Garcia, A.I. Real, Plastic films for agricultural applications, J. Plastic Film & Sheeting 22 (2006) 85–102.
[8] E. Klampaftis, D. Ross, K.R. McIntosh, B.S. Richards, Enhancing the performance of solar cells via luminescent down-shifting of the incident spectrum: a review, Sol. Energy Mater. Sol. Cells 93 (2009) 1182–1194.
[9] B.S. Richards, K.R. McIntosh, Overcoming the poor short wavelength spectral responses of CdS/CdTe photovoltaic modules via luminescence down-shifting: ray-tracing simulations, Prog. Photovoltaics 15 (2007) 27–34.
[10] X. Zhang, Y. Xiao, X. Qian, A ratiometric fluorescent probe based on FRET for imaging Hg^{2+} ions in living cells, Angew. Chem. Int. Ed. 47 (2008) 8025–8029.
[11] R.E. Martin, F. Diederich, Linear monodisperse (-conjugated oligomers: model compounds for polymers and more, Angew. Chem. Int. Ed. 38 (1999) 1350–1377.
[12] K.C. Moss, K.N. Bourdakos, V. Bhalla, K.T. Kamtekar, M.R. Bryce, M.A. Fox, H.L. Vaughan, F.B. Dias, A.P. Monkman, Tuning the intramolecular charge transfer emission from deep blue to green in ambipolar systems based on dibenzothiophene S,S-dioxide by manipulation of conjugation and strength of the electron donor units, J. Org. Chem. 75 (2010) 6771–6781.
[13] J.L. Segura, N. Martin, Functionalized oligoarylenes as building blocks for new organic materials, J. Mater. Chem. 10 (2000) 2403–2435.
[14] D.P. Hagberg, T. Marinado, K.M. Karlsson, K. Nonomura, P. Qin, G. Boschloo, T. Brinck, A. Hagfeldt, L. Sun, Tuning the HOMO and LUMO energy levels of organic chromophores for dye sensitized solar cells, J. Org. Chem. 72 (2007) 9550–9556.
[15] X. Tang, W. Liu, J. Wu, C.S. Lee, J. You, P. Wang, Synthesis, crystal structures, and photophysical properties of triphenylamine-based multicyano derivatives, J. Org. Chem. 75 (2010) 7273–7278.
[16] W. Lin, L. Yuan, Z. Cao, Y. Feng, J. Song, Through-bond energy transfer cassettes with minimal spectral overlap between the donor emission and acceptor absorption: coumarin-rhodamine dyads with large pseudo-Stokes shifts and emission shifts, Angew. Chem. Int. Ed. 49 (2010) 375–379.
[17] C.J. Brabec, C. Winder, N.S. Sariciftci, J.C. Hummelen, A. Dhanabalan, P.A. van Hal, R.A. Janssen, A low-bandgap semiconducting polymer for photovoltaic devices and infrared emitting diodes, Adv. Funct. Mater. 12 (2002) 709–712.
[18] F.L. Zhang, A. Gadisa, O. Inganas, M. Svensson, M.R. Andersson, Influence of buffer layers on the performance of polymer solar cells, Appl. Phys. Lett. 84 (2004) 3906–3908.
[19] M. Velusamy, K.R.J. Thomas, J.T. Lin, Y.-C. Hsu, K.-C. Ho, Organic dyes incorporating low-band-gap chromophores for dye-sensitized solar cells, Org. Lett. 7 (2005) 1899–1902.
[20] D. Deng, Y. Yang, J. Zhang, C. He, M. Zhang, Z.-G. Zhang, Z. Zhang, Y. Li, Triphenylamine-containing linear D-A-D molecules with benzothiadiazole as acceptor unit for bulk-heterojunction organic solar cells, Organic Electronics 12 (2011) 614–622.
[21] J.-Z. Cheng, C.-C. Lin, P.-T. Chou, A. Chaskar, K.-T. Wong, Fluorene as the (-spacer for new two-photon absorption chromophores, Tetrahedron 67 (2011) 734–739.
[22] A Guide to Recording Fluorescence Quantum Yields, Jobin Yvon Ltd.
[23] Gaussian 09, Revision A.01, M. J. Frisch, G. W. Trucks, H. B. Schlegel, G. E. Scuseria, M. A. Robb, J. R. Cheeseman, G., Scalmani, V., Barone, B., Mennucci, G. A. Petersson, H., Nakatsuji, M., Caricato, X., Li, H. P. Hratchian, A. F. Izmaylov, J., Bloino, G., Zheng, J. L. Sonnenberg, M., Hada, M., Ehara, K., Toyota, R., Fukuda, J., Hasegawa, M., Ishida, T., Nakajima, Y., Honda, O., Kitao, H., Nakai, T., Vreven, J. A. Montgomery, Jr., J. E. Peralta, F., Ogliaro, M., Bearpark, J. J. Heyd, E., Brothers, K. N. Kudin, V. N. Staroverov, R., Kobayashi, J., Normand, K., Raghavachari, A., Rendell, J. C. Burant, S. S. Iyengar, J., Tomasi, M., Cossi, N., Rega, J. M. Millam, M., Klene, J. E. Knox, J. B. Cross, V., Bakken, C., Adamo, J., Jaramillo, R., Gomperts, R. E. Stratmann, O., Yazyev, A. J. Austin, R., Cammi, C., Pomelli, J. W. Ochterski, R. L. Martin, K., Morokuma, V. G. Zakrzewski, G. A. Voth, P., Salvador, J. J. Dannenberg, S., Dapprich, A. D. Daniels, O., Farkas, J. B. Foresman, J. V. Ortiz, J. Cioslowski, and D. J. Fox, Gaussian, Inc., Wallingford CT, 2009.
[24] S.-I. Kato, T. Matsumoto, M. Shigeiwa, H. Gorohmaru, S. Maeda, T. Ishii, S. Mataka, Novel 2,1,3-benzothiadiazole-based red-fluorescent dyes with enhanced two-photon absorption cross-sections, Chem. Eur. J. 12 (2006) 2303–2307.
[25] Patent, WO01/49768.
[26] J.-J. Kim, H. Choi, J.-W. Lee, M.-S. Kang, K. Song, S.O. Kang, J. Ko, A polymer gel electrolyte to achieve ≥6% power conversion efficiency with a novel organic dye incorporating a low-band-gap chromophore, J. Mater. Chem. 18 (2008) 5223–5229.
[27] C.S. Li, Y.H. Tsai, W.C. Lee, W.J. Kuo, Synthesis and photophysical properties of pyrrole/polycyclic aromatic units hybrid fluorophores, J. Org. Chem. 75 (2010) 4004–4013.
[28] K. Ohta, Y. Chiba, T. Ogawa, Y. Endo, Promising core structure for nuclear receptor ligands: design and synthesis of novel estrogen receptor ligands based on diphenylamine skeleton, Bioorg. Med. Chem. Lett. 18 (2008) 5050–5053.
[29] H. Konno, S. Aimoto, S.O. Smith, K. Nosaka, K. Akaji, Synthesis of [19,35, 36-(13)C(3)]-labeled TAK779 as a molecular probe, Bioorg. Med. Chem. 17 (2009) 5769–5774.
[30] A. Pron, G. Zhou, H. Norouzi-Arasi, M. Baumgarten, K. Mullen, Controlling the charge transfer in phenylene-bridged borylene-amine pi-conjugated systems, Org. Lett. 11 (2009) 3550–3553.
[31] J. Svoboda, P. Stenclova, F. Uhlík, J. Zedník, J. Vohlídal, Synthesis and photophysical properties of α, (-bis(terpyridine)oligothiophenes, Tetrahedron 67 (2011) 75–79.
[32] I.B. Berlman, Empirical correlation between nuclear conformation and certain fluorescence and absorption characteristics of aromatic compounds, J. Phys. Chem. 74 (1970) 3085–3093.
[33] N.I. Nijegorodov, W.S. Downey, The influence of planarity and rigidity on the absorption and fluorescence parameters and intersystem crossing rate constant in aromatic molecules, J. Phys. Chem. 98 (1994) 5639–5643.
[34] H.L. Zhang, G. Zhao, Y. Ding, B. Wu, An efficient and enantioselective approach to the azaspirocyclic core of alkaloids: formal synthesis of halichlorine and pinnaic acid, J. Org. Chem. 70 (2005) 4954–4961.
[35] J.R. Lakowicz, Principles of Fluorescence Spectroscopy, 3rd edition, Springer Science+Business Media, NY, USA, 2006.
[36] F.B. Dias, S. Pollock, G. Hedley, L.O. Palsson, A. Monkman, I.I. Perepichka, I.F. Perepichka, M. Tavasli, M.R. Bryce, Intramolecular charge transfer assisted by conformational changes in the excited state of fluorene-dibenzothiophene-S,S-dioxide co-oligomers, J. Phys. Chem. B 110 (2006) 19329–19339.
[37] Z.R. Grabowski, K. Rotkiewicz, W. Rettig, Structural changes accompanying intramolecular electron transfer: focus on twisted intramolecular charge-transfer states and structures, Chem. Rev. 103 (2003) 3899–4032.
[38] J. Herbich, A. Kapturkiewicz, Electronic structure and molecular conformation in the excited charge transfer singlet states of 9-acridyl and other aryl derivatives of aromatic amines, J. Am. Chem. Soc. 120 (1998) 1014–1029.